Unveiling the Critical Role of Ion Coordination Configuration of Ether Electrolytes for High Voltage Lithium Metal Batteries

Shunqiang Chen, JiaJia Fan, Zhuangzhuang Cui, Lijiang Tan, Digen Ruan, Xin Zhao, Jinyu Jiang, Shuhong Jiao, Xiaodi Ren*

School of Chemistry and Materials Science, University of Science and Technology of China, Hefei 230026, China.

E-mail: xdren@ustc.edu.cn

Abstract: Ethers with distinctive reduction stability are emerging as the promising solution to the issues of lithium (Li) metal anode. However, their inferior oxidation stability (<4.0 V vs. Li/Li^+) cannot meet the ever-growing needs of high-voltage cathodes. Studies of ether electrolytes have been focusing on the archetype glyme structure with ethylene oxide moieties. Herein, we systematically vary the methylene units in the ether backbone and unveil the crucial effect of ion-ether coordination configuration on the electrolyte oxidation stability. The 1,3-dimethoxypropane (DMP, C3) molecule forms a unique six-membered chelating complex with Li^+, whose stronger solvating ability suppresses undesired oxidation side reactions. In addition, the favored hydrogen transfer reaction between DMP and salt anion induces a dramatic enrichment of LiF (a total atomic ratio of 76.7%) on the cathode surface. As a result, the DMP-based electrolyte demonstrates stable cycling of nickel-rich cathodes under a high voltage of 4.7 V (87% capacity retention after 150 cycles). This study offers fundamental insights into rational electrolyte design with wide electrochemical stability window for developing high-energy-density batteries.

Keywords: Ion coordination configuration; ether electrolytes; oxidation stability; lithium metal batteries; cathode-electrolyte interphase

Lithium (Li) metal is an ideal anode material because of its ultrahigh theoretical specific capacity (3860 mAh g^{-1}) and extremely low electrochemical potential (-3.04 V vs. standard hydrogen electrode)[1-4]. With high-voltage cathodes, Li-metal batteries (LMBs) could achieve much higher energy densities (~500 Wh kg^{-1}) than conventional Li-ion batteries (LIBs)[5]. Nevertheless, the implementation of LMBs is hindered by the highly reactive nature of Li metal causing uncontrollable parasitic reactions with electrolytes and the formation of Li dendrites resulting in safety issues. The conventional organic carbonate electrolytes for LIBs can form a stable solid-electrolyte interphase (SEI) on the graphite anode and remain stable with high-voltage cathodes (up to 4.5 V vs. Li/Li^+)[6]. Unfortunately, carbonate electrolytes have inherent high reactivity with Li metal, which would cause Li dendrite growth and low Coulombic efficiencies (CEs) for Li anode[7]. On the contrary, ether electrolytes with unique reduction stability are favorable for LMBs. However, ether electrolytes are still primarily used in low-voltage LMBs (e.g., Li-S, Li-O_2 batteries) due to their poor oxidation stability (<4.0 V vs. Li/Li^+)[8-10].

Recent studies have found that increasing the salt/solvent ratio is effective in tuning the electrochemical stability of ether-based electrolytes[11-12]. In high concentration electrolytes (HCEs)[13], anions enter the inner solvation sheath of Li^+ as there are an insufficient amount of solvent molecules to fully solvate Li^+ ions[14-17]. The preferred decomposition of anions and the resulting inorganic-rich electrode-electrolyte interphases could greatly improve the stabilities of both Li anode and high-voltage cathodes. HCEs based on 1,2-dimethoxyethane (DME), which is the most widely used ether solvent, have demonstrated good stability with layered cathodes[10]. Moreover, recent developments of localized high concentration electrolytes with non-solvating diluents (e.g., hydrofluoroethers) not only improve the physical properties of the electrolytes (e.g., viscosity, ionic conductivity, wettability, etc.) but also enhance the electrochemical stability of ether electrolytes[18-23]. However, recent studies have found the instability of DME-based electrolytes under higher voltages over 4.5 V[18]. For future applications of ether electrolytes, it is urgent to further improve the electrolyte oxidation stability on Ni-rich cathodes with reactive Ni^{3+}/Ni^{4+} surface sites.[24-25]

Apart from concentration adjustments, co-solvent[20] and additive screening[26-27], electrolyte molecular design offers unique capabilities for precise tuning of the electrolyte solvation structure and the interfacial reaction processes. Recently, ether molecules with electron-withdrawing

functional groups have demonstrated better oxidation stability with high-voltage cathodes. A series of multi-fluorinated linear ethers and cyclic ethers were shown to have enhanced electrochemical stabilities on both Li anode and high-voltage cathode[28-31]. Mono-chlorinated[32] and mono-fluorinated ethers[33] have also been introduced recently, which demonstrated enhanced stabilities on NMC811 cathodes. Nevertheless, from the perspective of economy and ecology, it is highly desirable to explore new molecular design strategies for developing non-fluorinated ether electrolytes with high oxidation stability.

In this work, we investigate the effect of ion-solvent coordination configuration on the electrochemical behavior of electrolytes by adjusting the length of the -$(CH_2)_n$- units of the linear ether molecular structure. Systematic variation of the ether backbone shows a profound influence on the Li^+-chelating behavior and the electrolyte electrochemical stability. Compared to DME, which is the archetype ether solvent with a five-membered chelate ring, 1,3-dimethoxypropane (DMP) was found to form a six-membered chelate ring with a stronger Li^+-solvation stability in the concentrated electrolyte, which significantly inhibits side reactions of labile free solvent molecules on the cathode. For 1,4-dimethoxybutane (DMB), the seven-membered chelate ring is not as stable and the ion coordination model changes from bidentate to monodentate with reduced oxidation stability. Importantly, the preferred hydrogen transfer reaction between DMP and salt anion induces the formation of a highly effective LiF-enriched cathode-electrolyte interphase (CEI). As a result, the DMP-based electrolyte demonstrates significantly enhanced performance on Ni-rich cathodes under a high voltage of 4.7 V with a capacity retention of 87% after 150 cycles. In addition, the DMP-based electrolyte also enables superior high-rate performance (4C or 8 mA cm^{-2}) and wide-temperature cycling stability (-20 to 50 ^oC). Our findings reveal the direct correlation of ether electrolyte chelate ring size with the electrochemical stability and provide new insights into electrolyte design for achieving high energy density battery systems.

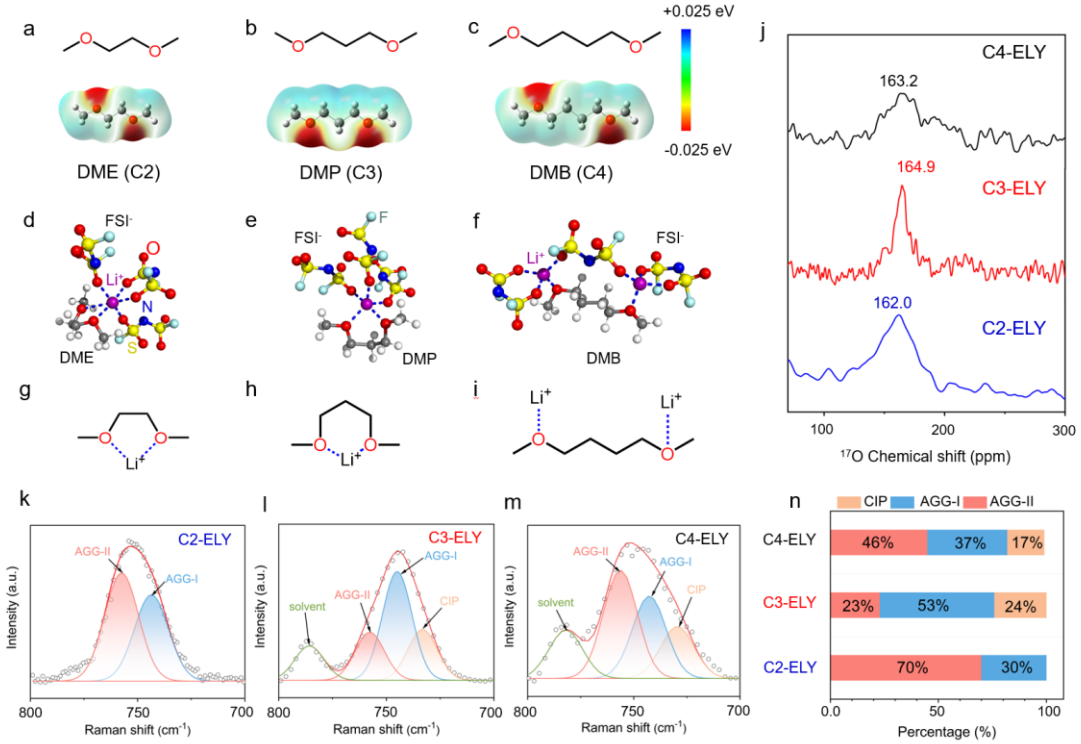

Figure 1. Characterizations of electrolyte solvation structures. Molecular structures and electrostatic potential maps of (a) DME (C2), (b) DMP (C3) and (c) DMB (C4). Ion solvation structures in (d, g) C2-ELY, (e, h) C3-ELY and (f, i) C4-ELY retrieved from MD simulations. (j) ^{17}O-NMR spectra of different electrolytes at 25^{o}C. (k-m) Raman spectra of different electrolytes. (n) The peak area ratios of CIP, AGG-I, and AGG-II in different electrolytes from the Raman spectra. Colour scheme of atoms: Li, purple; O, red; S, yellow; N, navy; H, white; C, dark grey and F, light blue.

We prepared the DME, DMP and DMB-based electrolytes with a high LiFSI/ether ratio of 1:1 (in molar ratio) and 1,1,2,2-tetrafluoroethyl-2,2,3,3-tetrafluorpropyl ether (TTE) as the diluent (ether: diluent=1:3 in molar ratio) to exploit the potential of ether-based electrolytes in high-voltage LMBs[15]. ^{1}H and ^{13}C-nuclear magnetic resonance (NMR) spectra of the solvents are shown in Figures S1-S4. Each of the three ether molecules has two oxygen (O) atoms as the Li^+ binding site, while the number of -CH_2- units in between is varied (Figures 1a-1c, along with the electrostatic potential map to show the negative charge density on O atoms for Li^+-binding). The three electrolytes are named C2-ELY, C3-ELY and C4-ELY, respectively, according to the number of -CH_2- units. Snapshots of electrolyte solvation structures from molecular dynamics simulations and the radial distribution function (RDF) plots are shown in Figures S5 and S6, which indicates that nearly all ether molecules are within the first Li^+ solvation sheath, while TTE only appears in the

outer solvation layer due to its negligible Li^+-solvating ability[17]. Nevertheless, the number of -CH_2- units shows a critical influence on the Li^+-solvent coordination structure in the concentrated solvation complex. In C2-ELY, the most populated Li^+ solvation structure represents a five-membered chelate ring configuration with two O atoms simultaneously binding to the Li^+ ion (Figures 1d, 1g and S7). A similar chelating effect could be found in C3-ELY, while the chelate ring size increases to six-membered (Figures 1e, 1h). However, in C4-ELY, the chelating effect disappears when the number of -CH_2- units reaches four, and only one oxygen atom in DMB participates in the solvation of the Li^+ ion (the other O atom solvates a nearby Li^+), as shown in Figures 1f and1i. Such monodentate coordination for DMB has also been suggested previously[28].

Raman spectroscopy was employed to probe the solvation feature of the FSI^- anion. As shown in Figures 1k-1m, the signals between 700-800 cm^{-1} come from the vibrations of the S-N-S bond in FSI^-, which has been commonly used to represent the binding feature between Li^+ and FSI^- in the electrolyte. The peaks around 733 cm^{-1}, 747 cm^{-1} and 757 cm^{-1} could be assigned to contact ion pairs (CIP) and ion aggregates-I (AGG-I, with FSI- binding to two Li^+ ions) and AGG-II (with FSI^- binding to more than two Li^+ ions), respectively (the peak at ~790 cm^{-1} comes from the DMP or DMB solvent)[34-36]. For the concentrated solvation complexes in C2-ELY, AGG-I and AGG-II are the dominant structures with close interactions between Li^+ and FSI^-. However, mainly AGG-I and CIP solvation complexes are found in C3-Ely, which suggests a relatively weak interaction between Li^+ and FSI^-. This is most likely due to the unique six-membered chelating ring configuration formed by DMP. The solvation structure in the C4-Ely is much more complicated than the other two, where CIP (17%), AGG-I (37%) and AGG-II (46%) show their co-existence. The enhanced Li^+-FSI^- interaction compared to that of DMP is likely due to the relatively weak monodentate binding of DMB to Li^+. However, we could not exclude the possibility of the temporary formation of a seven-membered chelate ring in the dynamic solvation structure, which may be related to the weak presence of CIP in C3-ELY. To gain further insight into the influence of the Li^+-solvent coordination configuration on the solvation structure, ^{17}O nuclear magnetic resonance (^{17}O-NMR) tests were carried out for the electrolytes (Figure 1j). Compared to C2-ELY and C4-ELY, the ^{17}O signal of FSI^- (164.9 ppm) in C3-ELY shifts toward the downfield. According to previous studies[37], this likely indicates a decreased ion-dipole interaction between FSI^- and Li^+ in the concentrated solvation

structure. In the meantime, a significant difference of the ^{17}O signal width was observed between the three electrolytes at room temperature. The apparently smaller peak width in the C3-ELY suggests FSI^- is more mobile in the electrolyte due to the favored binding configuration between DMP and Li^+, while the broad peaks in C2-ELY and C4-ELY indicate the stronger electrostatic interactions between FSI^- and Li^+. This could be further supported by the higher ion mobility in C3-ELY as obtained from the pulsed-field gradient (pfg)-NMR tests. As shown in Table S1, the self-diffusion coefficients of Li^+ and FSI^- in C3-ELY are nearly two times higher than those in the other two electrolytes. These results evidence the critical influence of the chelate ring size on the electrolyte solvation structure in the electrolytes. This is also different from the recent reports of 1,2-diethoxyethane (DEE) or 1,2-dimethoxypropane based electrolytes, which decrease the Li^+-solvation ability of solvents and promote Li^+-anion interactions with steric hindrance effects to enhance the anion reactivity[8, 38].

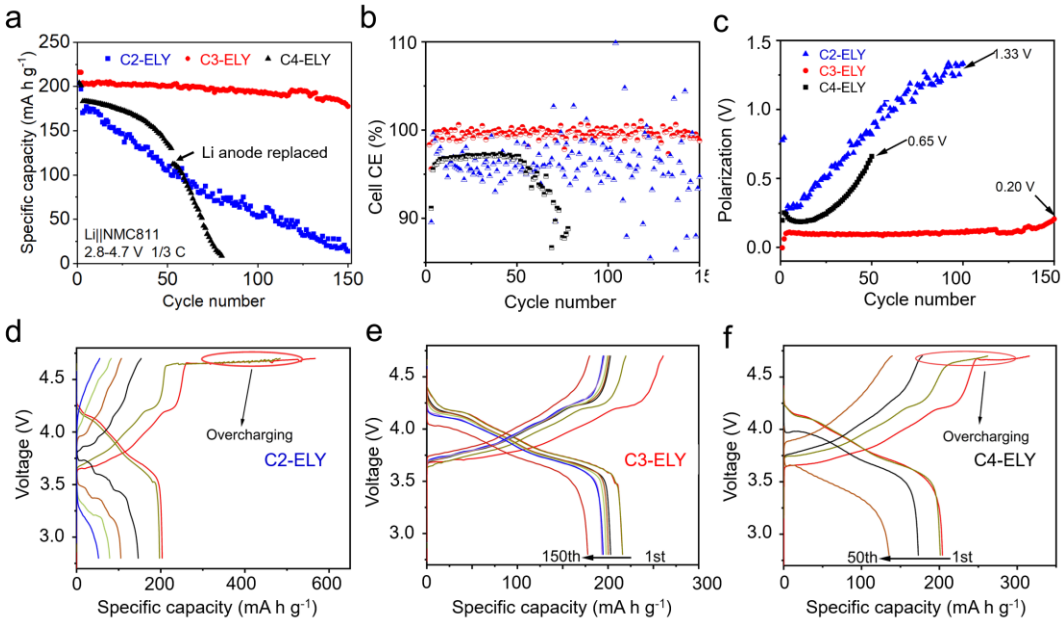

Figure 2. Electrochemical tests with different electrolytes. (a) Cycling performances, (b) cell CEs and (c) polarization of Li||scNMC811 cells using different electrolytes with a moderately high loading scNMC811 cathodes (2 mAh cm^{-2}) at 4.7 V cut-off voltage; Corresponding voltage profiles of the cells using (d) C2-ELY, (e) C3-ELY, (f) C4-ELY. The charge/discharge rates were C/10 for the two formation cycles and C/3 afterward.

In order to compare the electrochemical stability of electrolytes with different Li^+ chelate ring sizes, Li||NMC811cells were assembled and cycled within a wide potential range of 2.8-4.7 V. Single crystalline (sc) NMC811 cathode was chosen as the model cathode material to avoid interference from secondary particle cracking. Meanwhile, a similar stability trend for these electrolytes was demonstrated in the cells with polycrystalline (pc) NMC811 cathodes (Figures S8-S10). As shown in Figure 2, batteries with C2-ELY and C4-ELY show excessive electrolyte oxidation during charging in the first formation cycle (C/10 rate) and an apparent capacity drop after switching to a higher cycling rate (C/3). In C2-ELY, the capacity of the battery shows a linear decay trend and negligible capacity was retained after 150 cycles. In C4-ELY, the battery capacity was relatively stable for 20 cycles before a drastic capacity loss after 50 cycles. The battery capacity did not recover after a new Li anode was replaced, which supports that the capacity degradation is mainly due to the failure of the cathode. In both electrolytes, the low cell CEs suggest severe parasitic reactions between electrolytes and the high-voltage cathode. In sharp contrast, the Li||NMC811 cell with C3-ELY shows stable cycling (capacity retention of 87% after 150 cycles) and a high cell CE (~99.5%) under 4.7 V with no apparent over-charging observed. The DMP-based electrolyte also enables much smaller cell overpotential evolutions than those in the DME and DMB-based electrolytes, in agreement with its stable cycling performance (Figure 2c). Moreover, for direct comparison of different main solvents without the influence of the TTE diluent, HCEs based on the three ether solvents were also tested. The stable cycling performance in the DMP-based HCE further proves that the solvent structure is mainly responsible for the enhanced cathode stability under high voltages (Figure S11).

The leakage currents under high voltages are critical parameters for evaluating the oxidation stability of electrolytes on the NMC811 cathode surface (Figures 3a and S12)[1]. The cells were cycled for three cycles at C/10 rate before charged to 4.5 V, then held at a potential of 4.5 V and 4.6 V for 10 hours, respectively. Compared to C2-ELY and C4-ELY, the leakage current for C3-ELY reaches a minimum value of ~8.3 μA cm^{-2} (on pcNMC811) and ~5.6 μA cm^{-2} (on scNMC811) after 10 h at 4.6 V. Greatly suppressed leakage current was also observed in C3-ELY compared to those in C2-ELY and C4-ELY at 4.7 V, which also indicates the better oxidation stability of C3-ELY. In addition, the comparison of cell rate performance is shown in Figure S13. The C3-ELY electrolyte

exhibits excellent rate performance, in which specific capacities at 4C charge or discharge rates (or 8 mA cm^{-2} current density) are much higher than those in C2-ELY and C4-ELY. With the adjustment of -CH_2- units, the ionic conductivity increases from 1.70 to 4.33 and 5.90 mS cm^{-1} in the DME, DMP and DMB-based electrolytes, respectively (Figure S14). The relatively weak Li^+-FSI^- electrostatic interaction may contribute to the lower viscosity of C3-ELY (4.45 cP vs. 6.44 and 9.81 cP in C2-ELY and C4-ELY, respectively) (Table S2). Despite a higher viscosity, the C4-ELY has the highest ionic conductivity, which is likely due to the monodentate binding of DMB to Li^+ and the relatively easily hopping transport of Li^+. However, in C2-ELY and C4-ELY, electrolyte decompositions and corrosion of NMC811 cathodes could increase the cell polarization and decrease the reversible capacity. Under 1C or 2C charge and discharge cycling rate, the DMP-based electrolyte enables stable cycling without short-circuiting for about 200 cycles (1C, average cell CE~99.7%) and 150 cycles (2C, average cell CE>99.7%, respectively) (Figure S15). Moreover, the C3-ELY electrolyte enables stable operation with a wide temperature range (-20 to 50 ^oC) because of its favorable physical property and electrochemical stability (Figures S16-S17).

From post-mortem analysis, we confirm the crucial effect of ion-solvent coordination configuration on the oxidation stability of the ether electrolyte. As shown in Figure S18, no apparent change was observed when immersing the NMC811 cathode into the DME solvent after cycling in C3-ELY. In contrast, the cathodes cycled in C2-ELY and C4-ELY exhibit a light green and brown color, respectively, which indicates severe side reactions between the electrolytes and the cathode. This could be further verified by the morphology changes of cycled cathodes and the dissolution of transition metal ions in the electrolyte from inductively coupled plasma mass spectrometry (ICP-MS) results. The cycled NMC811 cathodes in C2-ELY and C4-ELY electrolytes show severe particle cracks (highlighted by red rectangles) while the cathode in C3-ELY remains intact after 100 cycles (Figure S19). Meanwhile, less transition metal ion depositions were observed on Li anodes cycled in C3-ELY (Figure S20). Compared to the other two ether-based electrolytes, the C3-ELY effectively inhibits electrolyte side reactions and preserves the integrity of the cathode after cycling under high voltages (4.7 V).

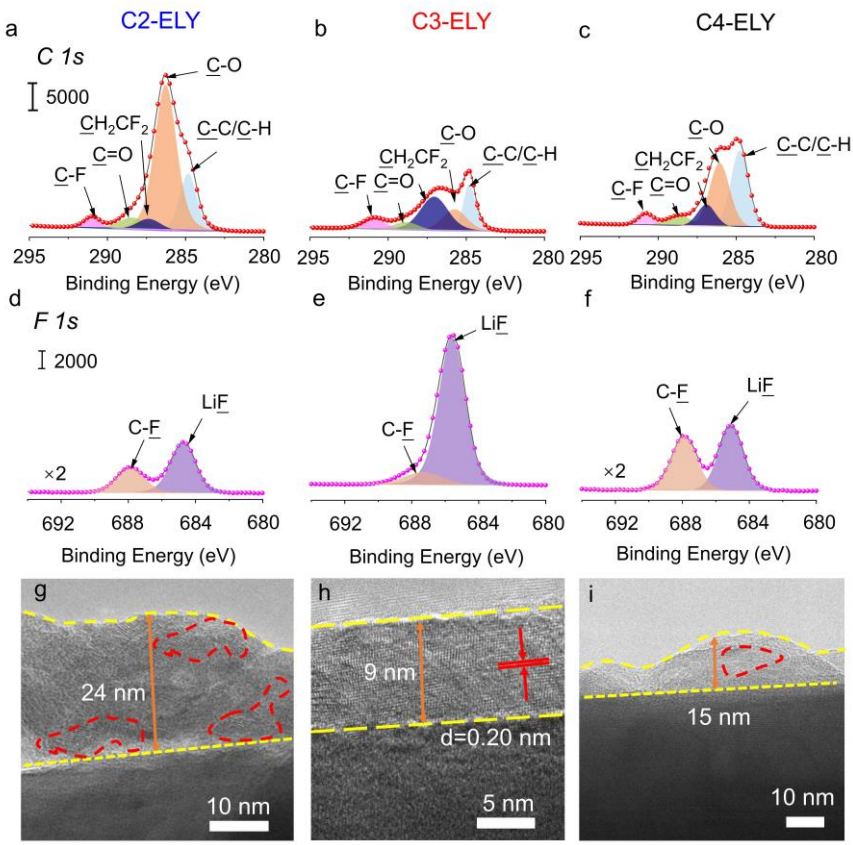

Figure 3. Characterizations of the CEIs. (a-c) C 1s and (d-e) F 1s XPS spectra of scNMC811 cathodes cycled for 100 cycles: (a, d) C2-ELY; (b, d) C3-ELY; (c, e) C4-ELY. (f-h) TEM images of cycled scNMC811 cathodes after 100 cycles: (f) C2-ELY; (g) C3-ELY; (h) C4-ELY.

X-ray photoelectron spectroscopy (XPS) analysis was conducted on cycled NMC811 cathodes to understand the difference of CEI compositions in the three electrolytes (Figure 3a-f). While similar species were observed in the CEIs due to the similarity of solvent structures, clear differences in their relative proportions reflect the critical influence of the chelate ring size on the electrochemical reactivity at the cathode surface. In the C 1s spectra, the surface of the cathodes cycled in C2-ELY and C4-ELY show stronger peaks of C-O at 286.0 eV, likely from excessive electrolyte decomposition. More importantly, the cathode in C3-ELY has a significantly stronger LiF signal in the F 1s spectrum (684.8 eV). The dramatic enrichment of LiF (Li and F atomic ratios of 43.5% and 33.2%, respectively) is critical for the greatly enhanced oxidation stability of the C3-ELY (Figure S21), since the high physical/chemical stability and low electronic conductivity of LiF make it a favorable interphase composition in various battery systems[8, 15]. The unusual LiF-enriched CEI has also been confirmed in a separate test (Figure S21g). Please note that the LiF formation is mainly from the FSI^- anion instead of the TTE molecule, as similar LiF enrichment could be

observed in the HCE-DMP without diluent (Figures S21d-f). The significant differences between the CEIs formed in these electrolytes were further characterized by transmission electron microscopy (TEM). TEM images reveal the formation of a thinner (~9 nm) CEI layer on the cathode surface in C3-ELY compared to those in C2-ELY (~24 nm) and C4-ELY (~15 nm) (Figure 3g-3i). Moreover, the CEI in C3-ELY has a high degree of crystallinity due to the enrichment of LiF (lattice spacing *d*~0.20 nm), while those in DME and DMB-based electrolytes are partially crystalline or nearly amorphous due to excessive electrolyte decomposition. Therefore, the critical influence of the ion coordination configuration on the electrolyte interfacial electrochemical reactions is verified.

To understand the underlying mechanism of the chelate ring size effect on the electrolyte oxidation stability and interfacial electrochemical behavior, we need to distinguish the role of Li^+-solvating solvent molecules and the non-solvating or "free" solvent molecules. Although from the perspective of the dynamic solvation structure in the liquid-phase electrolyte, they are indistinguishable due to the rapid exchange of solvent molecules between the solvating and the non-solvating state[39]. Nevertheless, their effects on the cathode stability could be largely different. Compared to free ether molecules, which are prone to be oxidized to generate corrosive side products[40], the Li^+-solvating ether molecules have enhanced oxidation stability due to reduced electron densities on their oxygen atoms[10, 41]. As discussed above, the ion coordination configuration has demonstrated a profound influence on the Li^+-solvating ability of ether molecules and the six-membered Li^+-DMP complex has the highest stability among the three ethers. Therefore, the probability of releasing the DMP molecule into a free state is the lowest, which would reduce the lifetime of free DMP molecules in the electrolyte (Figure 4a). In contrast, the lifetimes of free DME or DMB molecules would be much higher, which may induce more undesired solvent oxidation side reactions to corrode the cathode surface (Figure 3b). Furthermore, we examine the potential decomposition pathways of free ether molecules under high voltage using density functional theory (DFT) calculations. Previous studies have shown hydrogen (H)-transfer reactions between electrolyte components have a critical influence on the electrolyte reaction mechanism on the cathode[42-43]. Among different molecular complexes (solvent-anion, solvent-diluent, anion-diluent), the H-transfer reaction between solvent and anion was found to have the lowest oxidation potential[24, 40], possessing a prominent role during the CEI formation process. The adjustment of the $-CH_2-$ units

in the ether structure shows an apparent influence on their interaction with the FSI^- anion and the H-transfer reaction between solvent and anion, as shown in Figure 4b. Compared to the strong Li^+-solvent interaction, the interaction between solvent and anion is relatively weak[16]. However, it could strongly influence the charge-transfer reaction kinetics of the solvent-anion complex. FSI^- anion was found to have a higher binding affinity with DMP than DME and DMB. In addition, for all ether-anion complexes in the three electrolytes, the H-transfer reactions take place at the $-CH_2-$ group in the vicinity of the O atom (with the nitrogen (N) atom as the preferred proton acceptor). The oxidation potential of the DMP-FSI^- complex is lower than those of the DME-FSI^- and the DMB-FSI^- complexes, which suggests the reactivity depends on the distance between the two O atoms. This favored reaction between DMP and FSI^- could induce further decomposition of FSI^- and explain the formation of highly LiF-enriched CEI in C3-ELY (Figure 4a).

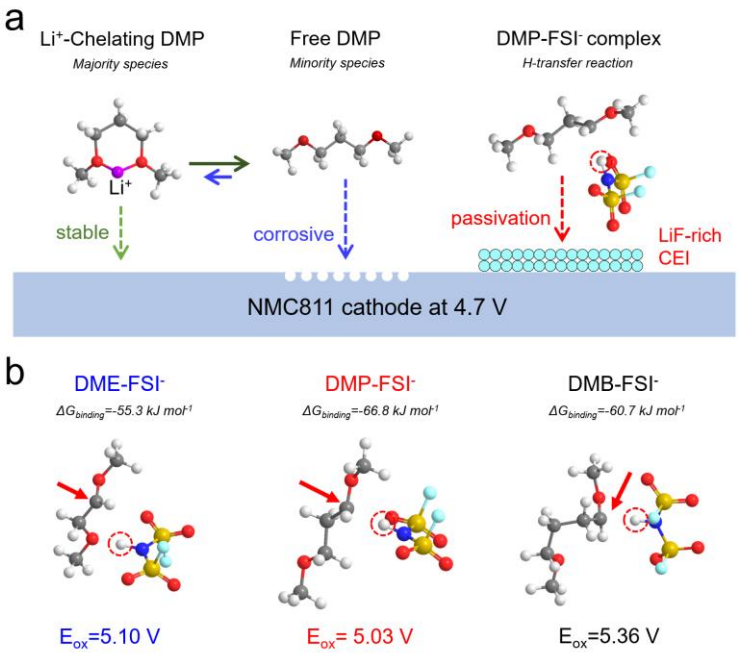

Figure 4. Proposed cathode interfacial reaction scheme. (a) Electrolyte species and their roles at the cathode surface. (b) The snapshots of anion-solvent complexes with H-transfer reactions.

Compared to the dramatic changes of electrolyte oxidation stability with the chelate ring size, its effect on the Li metal stability is less apparent. Li||Cu half cells were assembled to measure Li CEs.[44] For the full stripping method, all electrolytes exhibit similarly high CEs of ~99.3% over 400 cycles (Figure S22), which suggests the dominating role of anion reactions with the high salt/solvent

ratio in the electrolyte solvation structure[11, 19]. This is further supported by the similar XPS spectra of cycled Li||Li symmetric cells in different electrolytes (Figure S23). However, Li anodes retrieved from Li (50 μm thickness) ||NMC811 cells exhibit more apparent differences after cycling under high voltages. Top-view SEM images indicate the Li anode has a more uniform and compact morphology in the C3-ELY compared to those in C2-ELY and C4-ELY. The thickness of the Li anode in C3-ELY (~59 μm) is also the thinnest among the three (Figure S24-S26). We use electrochemical stripping to quantify the remaining active Li metal after cycling. As shown in Figure S25, the amount of active Li metal left is highest in C3-ELY, which corresponds to an average Li CE of 99.6%. With excellent electrochemical stability on both the cathode and the Li anode, the C3-ELY demonstrates greatly improved cycling stability under harsh conditions with high-loading cathode, thin Li anode and limited electrolyte (Figures S27 and S28). Therefore, the electrolyte oxidation stability and the crossover effect of cathode side products have a great influence on the Li anode reversibility in high-energy-density LMBs.

In summary, we prove the critical influence of the ion coordination configuration of ether molecules on the performance of 4.7 V high-voltage cathodes. In contrast to the typical five-membered chelate ring with Li^+, DMP forms a six-membered coordination configuration with a higher Li^+-binding stability to reduce the population of free solvent molecules and the accompanying oxidation side reactions. Furthermore, the DMP molecule has a higher affinity and preferred H-transfer reaction with the FSI^- anion to form a highly protective CEI enriched in LiF. As a result, the C3-ELY with a more suitable chelate ring exhibits greatly improved stability on NMC811 cathodes, compared to C2-ELY and C4-ELY. Our work illustrates the critical effect of Li^+-solvent configuration on the interfacial reaction landscape and adds a new dimension of knowledge in manipulating electrolyte solvation structure for future molecular design of electrolyte solvents.

Acknowledgements

This study was supported by the National Natural Science Foundation of China (Grant No.22179124, 21905265), the Fundamental Research Funds for the Central Universities (WK3430000007). The

numerical calculations in this paper have been done on the supercomputing system in the Supercomputing Center of the University of Science and Technology of China.

References

(1) Xue, W.; Huang, M.; Li, Y.; Zhu, Y. G.; Gao, R.; Xiao, X.; Zhang, W.; Li, S.; Xu, G.; Yu, Y.; Li, P.; Lopez, J.; Yu, D.; Dong, Y.; Fan, W.; Shi, Z.; Xiong, R.; Sun, C.-J.; Hwang, I.; Lee, W.-K.; Shao-Horn, Y.; Johnson, J. A.; Li, J., Ultra-High-Voltage Ni-Rich Layered Cathodes in Practical Li Metal Batteries Enabled by a Sulfonamide-Based Electrolyte. *Nat. Energy* **2021,** *6* (5), 495-505.

(2) Xue, W.; Gao, R.; Shi, Z.; Xiao, X.; Zhang, W.; Zhang, Y.; Zhu, Y. G.; Waluyo, I.; Li, Y.; Hill, M. R.; Zhu, Z.; Li, S.; Kuznetsov, O.; Zhang, Y.; Lee, W.-K.; Hunt, A.; Harutyunyan, A.; Shao-Horn, Y.; Johnson, J. A.; Li, J., Stabilizing Electrode-Electrolyte Interfaces to Realize High-Voltage Li||$LiCoO_2$ Batteries by a Sulfonamide-Based Electrolyte. *Energy Environ. Sci* **2021,** *14*, 6030-6040.

(3) Kim, M. S.; Zhang, Z.; Rudnicki, P. E.; Yu, Z.; Wang, J.; Wang, H.; Oyakhire, S. T.; Chen, Y.; Kim, S. C.; Zhang, W.; Boyle, D. T.; Kong, X.; Xu, R.; Huang, Z.; Huang, W.; Bent, S. F.; Wang, L. W.; Qin, J.; Bao, Z.; Cui, Y., Suspension Electrolyte with Modified Li^+ Solvation Environment for Lithium Metal Batteries. *Nat. Mater* **2022,** *21*, 445-454.

(4) Y. Yin, Y. Yang, D. Cheng, Mayer, M., Holoubek, Li. J, W., Raghavendran, G., A. Liu, B. Lu, Davies, D.M., Chen, Z. and Meng, Y. S. Fire-Extinguishing, Recyclable Liquefied Gas Electrolytes for Temperature-Resilient Lithium-Metal Batteries. *Nat. Energy* **2022,** *7*, 548-559.

(5) Qiao, Y.; Yang, H.; Chang, Z.; Deng, H.; Li, X.; Zhou, H., A High-Energy-Density and Long-Life Initial-Anode-Free Lithium Battery Enabled by a Li_2O Sacrificial Agent. *Nat. Energy* **2021,** *6* (6), 653-662.

(6) Ma, P.; Mirmira, P.; Amanchukwu, C. V., Effect of Building Block Connectivity and Ion Solvation on Electrochemical Stability and Ionic Conductivity in Novel Fluoroether Electrolytes. *ACS Cent Sci* **2021,** *7* (7), 1232-1244.

(7) Boyle, D. T.; Kim, S. C.; Oyakhire, S. T.; Vila, R. A.; Huang, Z.; Sayavong, P.; Qin, J.; Bao, Z.; Cui, Y., Correlating Kinetics to Cyclability Reveals Thermodynamic Origin of Lithium Anode Morphology in Liquid Electrolytes. *J Am Chem Soc* **2022**, *144*, 20717-20725.

(8) Chen, Y.; Yu, Z.; Rudnicki, P.; Gong, H.; Huang, Z.; Kim, S. C.; Lai, J. C.; Kong, X.; Qin, J.; Cui, Y.; Bao, Z., Steric Effect Tuned Ion Solvation Enabling Stable Cycling of High-Voltage Lithium Metal Battery. *J Am Chem Soc* **2021,** *143*, 18703-18713.

(9) Ren, X.; Zhang, X.; Shadike, Z.; Zou, L.; Jia, H.; Cao, X.; Engelhard, M. H.; Matthews, B. E.; Wang, C.; Arey, B. W.; Yang, X. Q.; Liu, J.; Zhang, J. G.; Xu, W., Designing Advanced In Situ Electrode/Electrolyte Interphases for Wide Temperature Operation of 4.5 V Li||LiCoO2 Batteries. *Adv Mater* **2020,** *32* (49), e2004898.

(10) Ren, X.; Zou, L.; Jiao, S.; Mei, D.; Engelhard, M. H.; Li, Q.; Lee, H.; Niu, C.; Adams, B. D.; Wang, C.; Liu, J.; Zhang, J.-G.; Xu, W., High-Concentration Ether Electrolytes for Stable High-Voltage Lithium Metal Batteries. *ACS Energy Lett* **2019,** *4* (4), 896-902.

(11) Cao, X.; Gao, P.; Ren, X.; Zou, L.; Engelhard, M. H.; Matthews, B. E.; Hu, J.; Niu, C.; Liu, D.; Arey, B. W.; Wang, C.; Xiao, J.; Liu, J.; Xu, W.; Zhang, J. G., Effects of Fluorinated Solvents on Electrolyte Solvation Structures and Electrode/Electrolyte Interphases for Lithium Metal Batteries. *Proc Natl Acad Sci U S A* **2021,** *118,* e2020357118.

(12) Fan, X.; Chen, L.; Ji, X.; Deng, T.; Hou, S.; Chen, J.; Zheng, J.; Wang, F.; Jiang, J.; Xu, K.; Wang, C., Highly Fluorinated Interphases Enable High-Voltage Li-Metal Batteries. *Chem* **2018,** *4* (1), 174-185.

(13) Jiao, S.; Ren, X.; Cao, R.; Engelhard, M. H.; Liu, Y.; Hu, D.; Mei, D.; Zheng, J.; Zhao, W.; Li, Q.; Liu, N.; Adams, B. D.; Ma, C.; Liu, J.; Zhang, J.-G.; Xu, W., Stable Cycling of High-Voltage Lithium Metal Batteries in Ether Electrolytes. *Nat. Energy* **2018,** *3* (9), 739-746.

(14) Suo, L.; Xue, W.; Gobet, M.; Greenbaum, S. G.; Wang, C.; Chen, Y.; Yang, W.; Li, Y.; Li, J., Fluorine-Donating Electrolytes Enable Highly Reversible 5-V-Class Li Metal Batteries. *Proc Natl Acad Sci U S A* **2018,** *115* (6), 1156-1161.

(15) Ren, X.; Zou, L.; Cao, X.; Engelhard, M. H.; Liu, W.; Burton, S. D.; Lee, H.; Niu, C.; Matthews, B. E.; Zhu, Z.; Wang, C.; Arey, B. W.; Xiao, J.; Liu, J.; Zhang, J.-G.; Xu, W., Enabling High-Voltage Lithium-Metal Batteries under Practical Conditions. *Joule* **2019,** *3* (7), 1662-1676.

(16) Wu, Z.; Li, R.; Zhang, S.; lv, L.; Deng, T.; Zhang, H.; Zhang, R.; Liu, J.; Ding, S.; Fan, L.; Chen, L.; Fan, X., Deciphering and Modulating Energetics of Solvation Structure Enables Aggressive High-Voltage Chemistry of Li Metal Batteries. *Chem* **2022,** *9*, doi.org/10.1016/j.chempr.2022.10.027.

(17) Ren, X.; Chen, S.; Lee, H.; Mei, D.; Engelhard, M. H.; Burton, S. D.; Zhao, W.; Zheng, J.; Li, Q.; Ding, M. S.; Schroeder, M.; Alvarado, J.; Xu, K.; Meng, Y. S.; Liu, J.; Zhang, J.-G.; Xu, W., Localized High-Concentration Sulfone Electrolytes for High-Efficiency Lithium-Metal Batteries. *Chem* **2018,** *4* (8), 1877-1892.

(18) Langdon, J.; Sim, R.; Manthiram, A., Gas Generation in Lithium Cells with High-Nickel Cathodes and Localized High-Concentration Electrolytes. *ACS Energy Lett.* **2022**, 2634-2640.

(19) Chen, S.; Zheng, J.; Yu, L.; Ren, X.; Engelhard, M. H.; Niu, C.; Lee, H.; Xu, W.; Xiao, J.; Liu, J.; Zhang, J.-G., High-Efficiency Lithium Metal Batteries with Fire-Retardant Electrolytes. *Joule* **2018,** *2* (8), 1548-1558.

(20) Jia, H.; Zou, L.; Gao, P.; Cao, X.; Zhao, W.; He, Y.; Engelhard, M. H.; Burton, S. D.; Wang, H.; Ren, X.; Li, Q.; Yi, R.; Zhang, X.; Wang, C.; Xu, Z.; Li, X.; Zhang, J. G.; Xu, W., High-Performance Silicon Anodes Enabled By Nonflammable Localized High-Concentration Electrolytes. *Advanced Energy Materials* **2019,** *9* (31), 1900784.

(21) Cao, X.; Ren, X.; Zou, L.; Engelhard, M. H.; Huang, W.; Wang, H.; Matthews, B. E.; Lee, H.; Niu, C.; Arey, B. W.; Cui, Y.; Wang, C.; Xiao, J.; Liu, J.; Xu, W.; Zhang, J.-G., Monolithic Solid-Electrolyte Interphases Formed in Fluorinated Orthoformate-Based Electrolytes Minimize Li Depletion and Pulverization. *Nat. Energy* **2019,** *4* (9), 796-805.

(22) Chen, S.; Nian, Q.; Zheng, L.; Xiong, B.-Q.; Wang, Z.; Shen, Y.; Ren, X., Highly Reversible Aqueous Zinc Metal Batteries Enabled by Fluorinated Interphases in Localized High Concentration Electrolytes. *J. Mater. Chem. A.* **2021,** *9* (39), 22347-22352.

(23) Lu, B.; Li, W.; Cheng, D.; Bhamwala, B.; Ceja, M.; Bao, W.; Fang, C.; Meng, Y. S., Suppressing Chemical Corrosions of Lithium Metal Anodes. *Adv. Energy Mater.* **2022**, 2202012.

(24) Ren, X.; Gao, P.; Zou, L.; Jiao, S.; Cao, X.; Zhang, X.; Jia, H.; Engelhard, M. H.; Matthews, B. E.; Wu, H.; Lee, H.; Niu, C.; Wang, C.; Arey, B. W.; Xiao, J.; Liu, J.; Zhang, J. G.; Xu, W., Role of Inner Solvation Sheath Within Salt-Solvent Complexes in Tailoring Electrode/Electrolyte Interphases for Lithium Metal Batteries. *Proc Natl Acad Sci U S A* **2020,** *117* (46), 28603-28613.

(25) Holoubek, J.; Liu, H.; Wu, Z.; Yin, Y.; Xing, X.; Cai, G.; Yu, S.; Zhou, H.; Pascal, T. A.; Chen, Z.; Liu, P., Tailoring Electrolyte Solvation for Li Metal Batteries Cycled at Ultra-Low Temperature. *Nat. Energy* **2021,** *6*, 303-313.

(26) Zhang, W.; Lu, Y.; Wan, L.; Zhou, P.; Xia, Y.; Yan, S.; Chen, X.; Zhou, H.; Dong, H.; Liu, K., Engineering a Passivating Electric Double Layer for High Performance Lithium Metal Batteries. *Nat. Commun.* **2022,** *13*, 2029–2040.

(27) Zhang, W.; Wu, Q.; Huang, J.; Fan, L.; Shen, Z.; He, Y.; Feng, Q.; Zhu, G.; Lu, Y., Colossal Granular Lithium Deposits Enabled by the Grain-Coarsening Effect for High-Efficiency Lithium Metal Full Batteries. *Adv Mater.* **2020,** *32* (24), e2001740.

(28) Yu, Z.; Wang, H.; Kong, X.; Huang, W.; Tsao, Y.; Mackanic, D. G.; Wang, K.; Wang, X.; Huang, W.; Choudhury, S.; Zheng, Y.; Amanchukwu, C. V.; Hung, S. T.; Ma, Y.; Lomeli, E. G.; Qin, J.; Cui, Y.; Bao, Z., Molecular Design for Electrolyte Solvents Enabling Energy-Dense and Long-Cycling Lithium Metal Batteries. *Nat. Energy* **2020,** *5* (7), 526-533.

(29) Yu, Z.; Rudnicki, P. E.; Zhang, Z.; Huang, Z.; Celik, H.; Oyakhire, S. T.; Chen, Y.; Kong, X.; Kim, S. C.; Xiao, X.; Wang, H.; Zheng, Y.; Kamat, G. A.; Kim, M. S.; Bent, S. F.; Qin, J.; Cui, Y.; Bao, Z., Rational Solvent Molecule Tuning for High-Performance Lithium Metal Battery Electrolytes. *Nat. Energy* **2022,** *7*, 94-106.

(30) Zhao, Y.; Zhou, T.; Ashirov, T.; Kazzi, M. E.; Cancellieri, C.; Jeurgens, L. P. H.; Choi, J. W.; Coskun, A., Fluorinated Ether Electrolyte with Controlled Solvation Structure for High Voltage Lithium Metal Batteries. *Nat Commun* **2022,** *13* (1), 2575.

(31) Amanchukwu, C. V.; Yu, Z.; Kong, X.; Qin, J.; Cui, Y.; Bao, Z., A New Class of Ionically Conducting Fluorinated Ether Electrolytes with High Electrochemical Stability. *J Am Chem Soc* **2020,** *142* (16), 7393-7403.

(32) Tan, L.; Chen, S.; Chen, Y.; Fan, J.; Ruan, D.; Nian, Q.; Chen, L.; Jiao, S.; Ren, X., Intrinsic Nonflammable Ether Electrolytes for Ultrahigh-Voltage Lithium Metal Batteries Enabled by Chlorine Functionality. *Angew Chem Int Ed Engl* **2022**, e202203693.

(33) Ruan, D.; Tan, L.; Chen, S.; Fan, J.; Nian, Q.; Chen, L.; Wang, Z.; and Ren, X. Solvent- vs. Anion-Chemistry: Unveiling the Structure-Dependent Reactivity in Tailoring Electrochemical Interphases for Lithium Metal Batteries. *JACS Au.*In press.

(34) Chen, X.; Zhang, Q., Atomic Insights into the Fundamental Interactions in Lithium Battery Electrolytes. *Acc Chem Res* **2020,** *53* (9), 1992-2002.

(35) Li, T.; Zhang, X. Q.; Yao, N.; Yao, Y. X.; Hou, L. P.; Chen, X.; Zhou, M. Y.; Huang, J. Q.; Zhang, Q., Stable Anion-Derived Solid Electrolyte Interphase by Regulating the Electrolyte Structure of Anions in Lithium Metal Batteries. *Angew Chem Int Ed Engl* **2021,** *133*, 22865-22869

(36) Jiang, L. L.; Yan, C.; Yao, Y. X.; Cai, W.; Huang, J. Q.; Zhang, Q., Inhibiting Solvent Co-Intercalation in a Graphite Anode by a Localized High-Concentration Electrolyte in Fast-Charging Batteries. *Angew Chem Int Ed Engl* **2021,** *60* (7), 3402-3406.

(37) Wan, C.; Hu, M. Y.; Borodin, O.; Qian, J.; Qin, Z.; Zhang, J.-G.; Hu, J. Z., Natural Abundance ^{17}O, ^{6}Li NMR and Molecular Modeling Studies of the Solvation Structures of Lithium Bis(fluorosulfonyl)imide/1,2-dimethoxyethane Liquid Electrolytes. *J. Power Sources.* **2016,** *307*, 231-243.

(38) Park, E.; Park, J.; Lee, K.; Zhao, Y.; Zhou, T.; Park, G.; Jeong, M.-G.; Choi, M.; Yoo, D.-J.; Jung, H.-G.; Coskun, A.; Choi, J. W., Exploiting the Steric Effect and Low Dielectric Constant of 1,2-Dimethoxypropane for 4.3 V Lithium Metal Batteries. *ACS Energy Lett.* **2022**, 179-188.

(39) Lee, K.-K.; Park, K.; Lee, H.; Noh, Y.; Kossowska, D.; Kwak, K.; Cho, M., Ultrafast Fluxional Exchange Dynamics in Electrolyte Solvation Sheath of Lithium Ion Battery. *Nat Commun* **2017,** *8*, 14658.

(40) Jang, D. H.; Oh, S. M., Electrolyte Effects on Spinel Dissolution and Cathodic Capacity Losses in 4 V $Li/Li_xMn_2O_4$ Rechargeable Cells. *J. Electrochem. Soc*. **1997**, *144*, 3342..

(41) Yamada, Y.; Wang, J.; Ko, S.; Watanabe, E.; Yamada, A., Advances and Issues in Developing Salt-Concentrated Battery Electrolytes. *Nat. Energy* **2019,** *4* (4), 269-280.

(42) Fadel, E. R.; Faglioni, F.; Samsonidze, G.; Molinari, N.; Merinov, B. V.; Goddard, W. A., III; Grossman, J. C.; Mailoa, J. P.; Kozinsky, B., Role of solvent-anion charge transfer in oxidative degradation of battery electrolytes. *Nat Commun* **2019,** *10* (1), 3360.
(43) Borodin, O.; Ren, X.; Vatamanu, J.; von Wald Cresce, A.; Knap, J.; Xu, K., Modeling Insight into Battery Electrolyte Electrochemical Stability and Interfacial Structure. *Acc Chem Res* **2017,** *50* (12), 2886-2894.
(44) Adams, B. D.; Zheng, J.; Ren, X.; Xu, W.; Zhang, J. G., Accurate Determination of Coulombic Efficiency for Lithium Metal Anodes and Lithium Metal Batteries. *Adv. Energy Mater.s* **2017,** *8* (7), 1702097.